

# Surface spin polarization in the magnetic response of GeTe Rashba ferroelectric.

A.A. Avakyants,<sup>1</sup> N.N. Orlova,<sup>1</sup> A.V. Timonina,<sup>1</sup> N.N. Kolesnikov,<sup>1</sup> and E.V. Deviatov<sup>1</sup>

<sup>1</sup>*Institute of Solid State Physics of the Russian Academy of Sciences,  
Chernogolovka, Moscow District, 2 Academician Ossipyan str., 142432 Russia*

(Dated: November 21, 2023)

We experimentally investigate magnetization reversal curves for a GeTe topological semimetal. In addition to the known lattice diamagnetic response, we observe narrow magnetization loop in low fields, which should not be expected for non-magnetic GeTe. The hysteresis is unusual, so the saturation level is negative in positive fields, and the loop is passed clockwise, in contrast to standard ferromagnetic behavior. The experimental hysteresis curves can not be obtained from usual ferromagnetic ones by adding/subtracting of any linear dependence, or even by considering several interacting magnetic phases. The possibility of several phases is also eliminated by the remanence plots technique (Henkel or  $\delta M$  plots). We explain our results as a direct consequence of the correlation between ferroelectricity and spin-polarized surface states in GeTe, similarly to magnetoelectric structures.

## I. INTRODUCTION

Recent renewal of interest to semimetals is mostly connected with topological effects. Topological semimetals are conductors with gapless electronic excitations with band touching in some distinct points, which are protected by topology and symmetry<sup>1</sup>. Similarly to topological insulators<sup>2</sup> and quantum Hall systems<sup>3,4</sup>, topological semimetals have topologically protected surface states. In Weyl semimetals (WSM) every band touching point splits into two Weyl nodes with opposite chiralities due to the time reversal or inversion symmetries breaking. As a result, Fermi arc surface states connect projections of Weyl nodes on the surface Brillouin zone and these surface states inherit the chiral property of the Chern insulator edge states<sup>1</sup>.

Usually, spin textures are known in magnetic materials as surface skyrmions<sup>5–13</sup> or spin helix structures<sup>14,15</sup>. For the magnetic WSMs (broken time reversal symmetry), the Fermi arc surface states were directly visualized in  $\text{Co}_3\text{Sn}_2\text{S}_2$  by scanning tunneling spectroscopy<sup>16</sup>. Surface topological textures were visualized in some magnetic semimetals by STM, Lorenz electron microscopy, and magnetic force microscopy<sup>17–19</sup>. Recent investigations show topological protection of skyrmion structures due to their origin from the spin-polarized topological surface states<sup>20</sup>.

However, spin textures due to the spin polarization of the Fermi arcs should also take place in nonmagnetic WSMs with broken inversion symmetry. Spin- and angle- resolved photoemission spectroscopy technique has demonstrated spin-polarized surface Fermi arcs<sup>21,22</sup>. Spin-orbit interaction lifts the spin degeneracy of the surface states leading to their in-plane spin polarization, with strongly correlated and predominantly antiparallel spin textures in the neighboring Fermi arcs<sup>23</sup>. As an example of nonmagnetic WSM, spin polarization of the arcs reaches 80%, as it has been discovered in TaAs<sup>24</sup>.

Among nonmagnetic WSM materials, GeTe is of special interest<sup>25–27</sup> due to the reported giant Rashba split-

ting<sup>27–30</sup>. GeTe is predicted to be topological semimetal in ferroelectric  $\alpha$ -phase<sup>31,32</sup>. Nonlinear Hall effect has been demonstrated in GeTe<sup>33</sup>, which is the direct manifestation of finite Berry curvature in topological media<sup>34</sup>. The direct measurement of the Rashba-split surface states of  $\alpha$ -GeTe(111) has been experimentally realized thanks to K doping<sup>35</sup>. It has been shown that the surface states are not the result of band bending and that they are decoupled from the bulk states. The giant Rashba splitting of the surface states of  $\alpha$ -GeTe is largely arising from the inversion symmetry breaking in the bulk<sup>35</sup>. Also, direct correlation between ferroelectricity and spin textures was demonstrated in GeTe<sup>36</sup>.

Surface spin polarization have been directly demonstrated in a magnetic response of topological semimetals with broken time-reversal symmetry<sup>37,38</sup>. Thus, one can expect a complicated response of a topological semimetal GeTe on the external magnetic field due to the spin polarization of topological surface states.

Here, we experimentally investigate magnetization reversal curves for a GeTe topological semimetal. In addition to the known lattice diamagnetic response, we observe narrow magnetization loop in low fields, which should not be expected for non-magnetic GeTe. We explain our results as a direct consequence of the correlation between ferroelectricity and spin-polarized surface states in GeTe, similarly to magnetoelectric structures.

## II. SAMPLES AND TECHNIQUE

GeTe single crystals were grown by physical vapor transport in the evacuated silica ampule. The initial GeTe load was synthesized by direct reaction of the high-purity (99.9999%) elements in vacuum. For the crystals growth, the obtained GeTe serves as a source of vapors: it was melted and kept at 770–780° C for 24 h. Afterward, the source was cooled down to 350° C at the 7.5 deg/h rate. GeTe crystals grew during this process on the cold ampule walls above the source.

The GeTe composition is verified by energy-dispersive

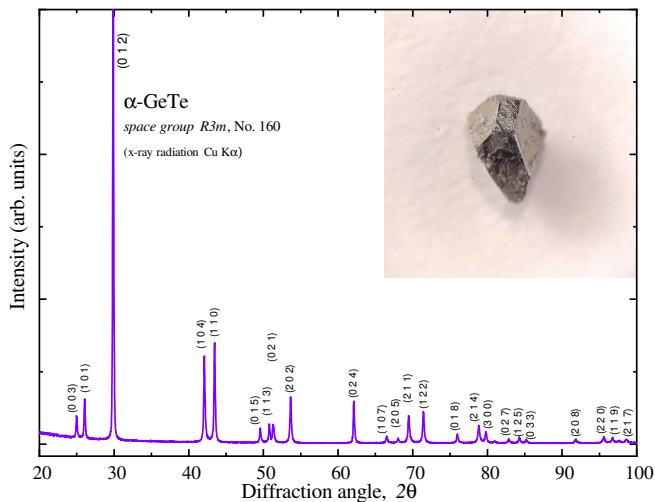


FIG. 1. (Color online) (a) The X-ray powder diffraction pattern (Cu  $K\alpha$  radiation), which is obtained for the crushed GeTe single crystal. The single-phase  $\alpha$ -GeTe is confirmed with the space group R3m (No.160). The inset shows optical image of the crystal.

X-ray spectroscopy. The powder X-ray diffraction analysis confirms single-phase GeTe, see Fig. 1 (a), the known structure model<sup>28</sup> is also refined with single crystal X-ray diffraction measurements. Ferroelectric polarization and Rashba splitting are defined by the non-centrosymmetric distorted rhombohedral structure ( $\alpha$ -GeTe) with space group R3m (No. 160)<sup>28</sup>. For our GeTe single crystals, giant Rashba splitting<sup>28</sup> has been confirmed in capacitance measurements<sup>27</sup>.

To investigate magnetic properties, we use Lake Shore Cryotronics 8604 VSM magnetometer, equipped with nitrogen flow cryostat. The topological semimetals are essentially three-dimensional objects<sup>1</sup>, so we have to select relatively thick (above  $0.5 \mu\text{m}$ ) mechanically exfoliated GeTe flakes. A small (0.82–9.54 mg) flake is mounted to the sample holder by low temperature grease, which has been tested to have a negligible magnetic response.

We investigate sample magnetization by standard method of the magnetic field gradual sweeping between two opposite field values to obtain magnetization loops. Also, the remanence plots technique (i.e., Henkel or  $\delta M$  plots) is routinely used to evaluate interactions between nanoparticles or grains<sup>39–41</sup>.

The technique is based on the comparison of the isothermal remanent magnetization curve (IRM,  $M_r$ ), and the DC demagnetization remanence curve (DCD,  $M_d$ ). The IRM curve is obtained on an initially demagnetized sample by applying a positive magnetic field. The DCD curve is measured by first saturating the sample and then measuring the remanence magnetization after application of progressively larger fields of opposite direction. For a system of noninteracting single-domain particles with uniaxial anisotropy, the IRM and DCD

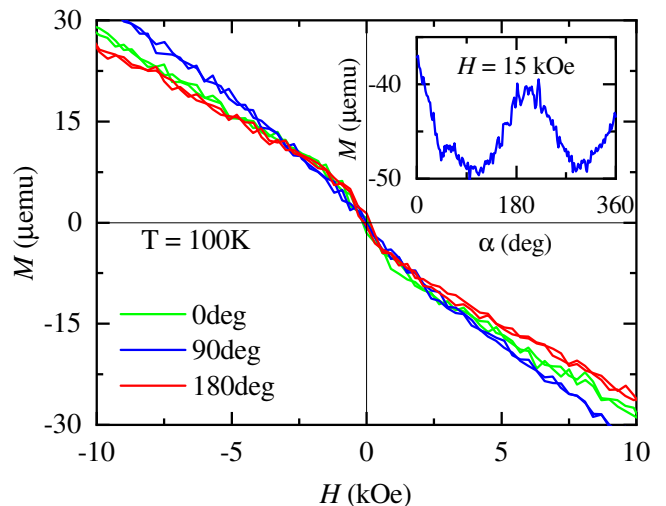


FIG. 2. (Color online) Magnetization curves at 100 K temperature for the 6.69 mg GeTe flake. The overall  $M(H)$  behavior shows diamagnetic response<sup>44</sup>, which is accompanied by the clearly visible kink in  $M(H)$  dependence at low fields, within  $\pm 1$  kOe interval. The  $M(H)$  curves are shown for several angles  $\alpha$  between the sample holder and magnetic field. Inset shows  $M(\alpha)$  dependence: we observe about 20% modulation of the  $M(\alpha)$  with  $180^\circ$  periodicity in the magnetic field 15 kOe. This shallow angle dependence seems to originate from the shape of the exfoliated flake with well-developed cleaved surface.

are related to each other via the Wohlfarth equation

$$M_d(H) = M_{rs} - 2M_r(H)$$

where  $M_{rs}$  is the saturation remanence and  $H$  is the applied magnetic field.

The  $\delta M$  or Henkel plot is a direct measure of the deviation from the linearity:

$$\delta M(H) = M_d(H) - [M_{rs} - 2M_r(H)]$$

Interparticle interactions are detected through the appearance of a negative dip (demagnetizing interactions, typically dipolar one) or a positive peak (magnetizing, usually exchange, interactions) in the  $\delta M$  plots, whereas  $\delta M = 0$  has generally been taken as an indication of the absence of interactions<sup>40,42</sup>. In other words, positive and negative  $\delta M$  contributions indicate more than one phase<sup>43</sup>.

### III. EXPERIMENTAL RESULTS

Fig. 2 shows magnetization loops at 100 K temperature for the 6.69 mg GeTe flake. The overall  $M(H)$  behavior shows the diamagnetic response, which is known for the bulk GeTe mostly due to the lattice<sup>44</sup>. From the linear diamagnetic dependence we can estimate the slope as  $-3 \cdot 10^{-6} \text{ emu/cm}^3$ , this estimation well corresponds to

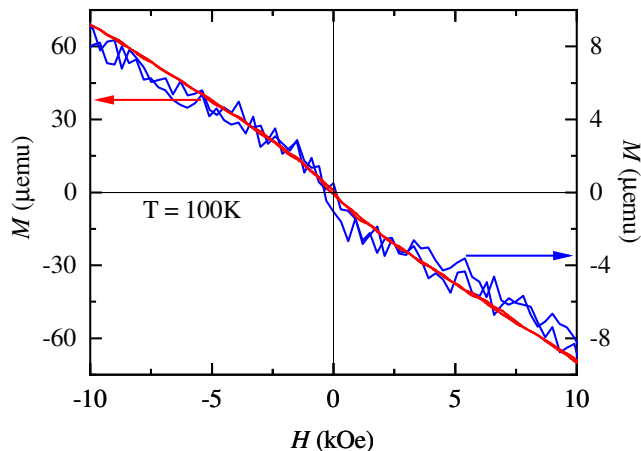


FIG. 3. (Color online) Magnetization loops at 100 K temperature for two 9.54 mg and 0.82 mg GeTe flakes, see the left and the right axes, respectively. The diamagnetic slope scales with the sample mass. The linear curves with low-field kink are qualitatively similar to the behavior in Fig. 2. The low-field kink is better seen for the smaller sample, so even low-field hysteresis can be seen for the smallest 0.82 mg GeTe flake.

the reported GeTe volume susceptibility<sup>44</sup>. The  $M(H)$  curves show some angle dependence, as it is confirmed by the direct  $M(\alpha)$  measurement in the inset to Fig. 2: we observe about 20% modulation of the  $M(\alpha)$  with 180° periodicity in the magnetic field 15 kOe. This shallow angle dependence seems to originate from the shape of the exfoliated flake with well-developed cleaved surface.

The most striking experimental result is the clearly visible kink in  $M(H)$  dependence at low fields, within  $\pm 1$  kOe interval, see Fig. 2. The kink can be seen for any sample orientation. Diamagnetic response with low-field kink can be qualitatively reproduced for different GeTe flakes. For example, Fig. 3 shows  $M(H)$  curves for 9.54 mg and 0.82 mg samples, see the left and the right axes, respectively. We should conclude, that the standard linear diamagnetic response is accompanied by narrow magnetization loop, which should not be the case for the diamagnetic GeTe.

The diamagnetic slope scales with the sample mass, as it should be expected for the lattice-induced response: it is increased in approximately two times for the 1.5 mass increase, cp. Fig. 2 and Fig. 3, left axis; also, the slopes differ in 8 times for two flakes in Fig. 3, which is near the sample mass ratio 11.6. The  $\approx 25\%$  discrepancy can be ascribed to the different shape of the exfoliated flakes, due to the arbitrary orientation of the cleaved surfaces (cp. with the 20% modulation of the  $M(\alpha)$  in the inset to Fig. 2).

The low-field kink is better seen for the smaller samples, so even low-field hysteresis can be seen for the smallest 0.82 mg GeTe flake in Fig. 3. The hysteresis is shown in detail in Fig. 4 for all three samples. We use curve averaging (8 curves) to increase the signal/noise ratio. The

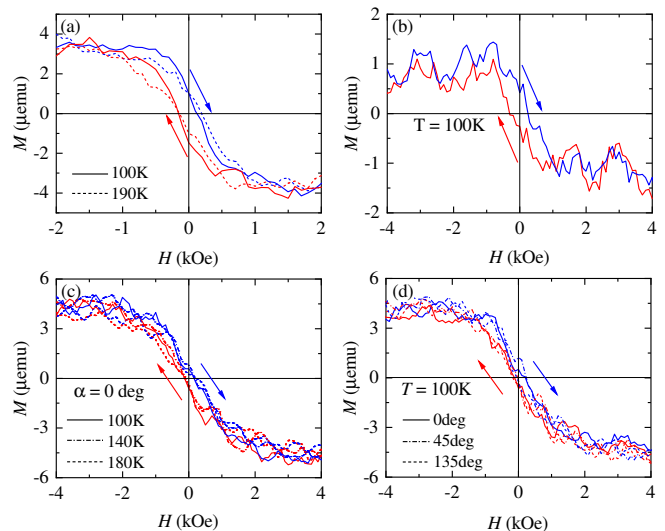


FIG. 4. (Color online) The low-field hysteresis region for all three samples. For every field sweep direction, we use curve averaging (8 curves) to increase the signal/noise ratio. The diamagnetic slope is subtracted from the averaged curves to highlight the nonlinear low-field behavior. (a) Curves for the 6.69 mg GeTe flake at two temperatures, 100 K (solid) and 190 K (dash). (b)  $M(H)$  curves for the smallest, 0.82 mg GeTe flake, at 100 K. (c-d) Hysteresis for the 9.54 mg flake at different temperatures (c) and sample orientation (d). For every sample, the saturation level is negative in positive fields, and the loop is passed clockwise, in contrast to usual ferromagnetic hysteresis.

linear diamagnetic slope is subtracted from the averaged curves to highlight the nonlinear low-field behavior.

First of all, all three samples show clear low-field hysteresis in Fig. 4. To our surprise, the saturation level is negative in positive fields, and the loop is passed clockwise, in contrast to usual ferromagnetic hysteresis. We wish to note, that the experimental curves in Fig. 4 can not be continuously transformed to the standard ferromagnetic one (the saturation level is positive in positive fields) by adding/subtracting of any linear dependence: the linear diamagnetic curve, been subtracted from the magnetization loop, can not invert the saturation levels around the zero field. This even qualitatively excludes any possible contribution from the sample holder, nitrogen atmosphere, and so on.

The saturation level value monotonically depends on the sample mass in Fig. 4 (a) and (c): it is increased from 3  $\mu\text{emu}$  in (a), for the 6.69 mg GeTe flake, to 4.5  $\mu\text{emu}$  in (c), for the 9.54 mg one. It is below 1  $\mu\text{emu}$  in (b), for the smallest, 0.82 mg GeTe flake, but the signal is noisy here. The hysteresis width at zero  $M$  level (coercivity) is different for all three samples, but no reasonable dependence can be seen in Fig. 4 (a-c). The hysteresis is not sensitive to temperature below 200 K, as it is shown in Fig. 4 (a) and (c). After subtracting the diamagnetic slope, the low-field hysteresis is not sensitive to the field

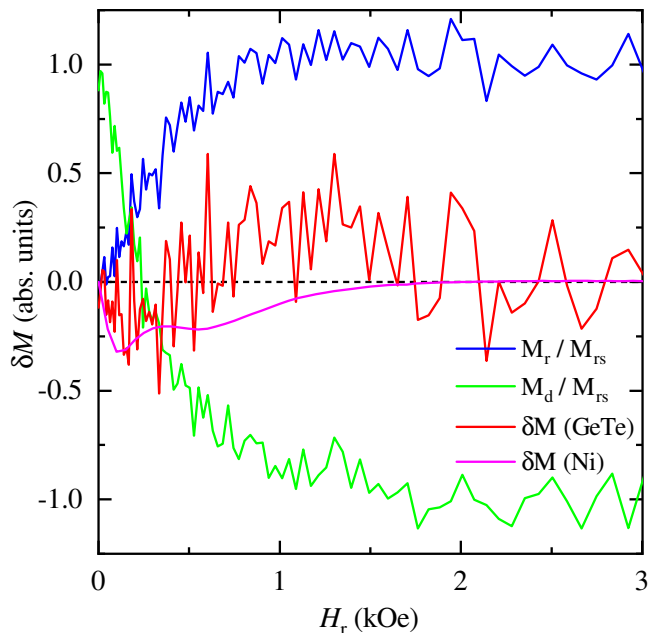


FIG. 5. (Color online) Henkel or remanence  $\delta M$  plot for 6.69 mg GeTe flake at 100 K temperature. The initial  $M_r(H), M_d(H)$  curves (blue and green ones, respectively), give the  $\delta M(H)$  (red) curve. Within the accuracy of experiment,  $\delta M(H)$  behavior can not definitely confirm several magnetic phases for our GeTe flakes. For comparison, a reference fully negative  $\delta M$  curve (magenta) is shown, as obtained for the standard nickel sample.

orientation within our accuracy, see Fig. 4 (d).

In principle, the hysteresis in Fig. 4 could be connected with several (at least two) interacting magnetic phases. This can be verified by the remanence plots technique (i.e., Henkel or  $\delta M$  plots), see Fig. 5. Positive and negative  $\delta M$  contributions indicate more than one phase<sup>43</sup>, whereas  $\delta M = 0$  has generally been taken as an indication of the absence of interphase interactions<sup>40,42</sup>.

Fig. 5 shows both the initial  $M_r(H), M_d(H)$  curves and the calculated  $\delta M(H)$ .  $\delta M(H)$  for GeTe varies around zero within the accuracy of experiment. Fig. 5 also shows a reference  $\delta M$  curve, obtained for the standard nickel sample. In the latter case, negative  $\delta M$  dip corresponds to the dipolar interaction between domains. Thus, the remanence plots technique can not definitely confirm several magnetic phases for our GeTe flakes.

#### IV. DISCUSSION

As a result, we observe that the lattice diamagnetic response is accompanied by the low-field hysteresis loop in GeTe. In contrast to usual ferromagnetic hysteresis, the saturation level is negative in positive fields so the loop is passed clockwise.

This hysteresis can not be obtained from standard ferromagnetic one even by considering several interact-

ing magnetic phases. In the latter case the bias field can move the magnetization switching even across the zero, so the magnetization loop is passed clockwise<sup>37</sup> (in contrast to single-phase ferromagnet with usual counterclockwise hysteresis). However, the bias field can not invert the saturation levels. Also, the remanence plots technique (i.e., Henkel or  $\delta M$  plots) does not confirm several magnetic phases for our GeTe flakes.

Even qualitatively, one can not also find two interacting magnetic phases in GeTe. One of the phases could be the spin textures from the surface states<sup>35</sup> in  $\alpha$ -GeTe(111). As it has been shown before, spin-polarized surface states can, in principle, give significant contribution into the overall magnetic response<sup>37,38</sup>. The second phase is the ferromagnetic bulk in magnetic topological semimetals<sup>37</sup>, but it can not be expected for the diamagnetic GeTe.

Also, GeTe composition is verified by energy-dispersive X-ray spectroscopy and the powder X-ray diffraction analysis. The obtained volume susceptibility  $-3 \cdot 10^{-6}$  well corresponds to the known values<sup>44</sup>. Thus, there is no magnetic impurities in our GeTe crystals.

On the other hand, correlation between the Rashba-split surface states<sup>35</sup> and ferroelectricity in  $\alpha$ -GeTe can be responsible for the observed hysteresis. Both the giant Rashba splitting of the surface states and bulk ferroelectricity are largely arising from the inversion symmetry breaking<sup>35</sup>. For our GeTe single crystals, giant Rashba splitting<sup>28</sup> and bulk ferroelectricity have been confirmed in capacitance measurements<sup>27</sup>. Direct correlation between ferroelectricity and spin textures was demonstrated in GeTe<sup>36</sup>. Thus, GeTe single crystal can be considered as magnetoelectric heterostructure<sup>45,46</sup> or multiferroic system<sup>47</sup>.

In magnetoelectrics, due to the coupling among the different degrees of freedom (ferroelectricity, ferromagnetism, or ferroelasticity) leading to these ordered states, the order parameter of one state can be controlled by tuning parameters different from their conjugate variable<sup>47</sup>. In the conditions of our experiment, variation of the magnetic field leads to appearance of the electric field due to the magnetoelectric coupling<sup>48</sup>. Electric field affects spin textures in GeTe<sup>36,46</sup>, which, subsequently, affects magnetization response<sup>37,38</sup>. As a result, the net magnetization follows the external field with some delay, producing the unusual hysteresis around zero field. This effect can be clearly seen only for significant diamagnetic response in GeTe, where it can not be mixed with usual ferromagnetic loop. Thus, unusual low-field hysteresis is a direct consequence of correlation between ferroelectricity and spin-polarized surface states in GeTe.

#### V. CONCLUSION

As a conclusion, we experimentally investigate magnetization reversal curves for a GeTe topological semimetal. In addition to the known lattice diamagnetic response, we

observe narrow magnetization loop in low fields, which should not be expected for non-magnetic GeTe. The hysteresis is unusual, so the saturation level is negative in positive fields, and the loop is passed clockwise, in contrast to standard ferromagnetic behavior. The experimental hysteresis curves can not be obtained from usual ferromagnetic ones by adding/subtracting of any linear dependence, or even by considering several interacting magnetic phases. The possibility of several phases is also eliminated by the remanence plots technique (Henkel or  $\delta M$  plots). We explain our results as a direct consequence of the correlation between ferroelectricity and

spin-polarized surface states in GeTe, similarly to magnetoelectric structures.

## ACKNOWLEDGMENTS

We wish to thank S.S Khasanov for X-ray sample characterization. We gratefully acknowledge financial support by the Russian Science Foundation, project RSF-23-22-00142, <https://rscf.ru/project/23-22-00142/>.

- 
- <sup>1</sup> As a recent review see N. P. Armitage, E. J. Mele, and Ashvin Vishwanath, *Reviews of Modern Physics* (2017), arXiv:1705.01111
  - <sup>2</sup> M. Z. Hasan and C. L. Kane, *Rev. Mod. Phys.* **82**, 3045 (2010).
  - <sup>3</sup> M. Büttiker, *Phys. Rev. B* **38**, 9375 (1988).
  - <sup>4</sup> E. V. Deviatov, *Physics-Uspexhi* **50** (2) 197 (2007).
  - <sup>5</sup> Wang, S.-X., Chang, H.-R. and Zhou, *J. Physical Review B* **96**, 115204 (2017).
  - <sup>6</sup> Chang, H.-R., Zhou, J., Wang, S.-X., Shan, W.-Y. and Xiao, D. *Physical Review B* **92**, 241103 (2015).
  - <sup>7</sup> Valizadeh, M. M. *International Journal of Modern Physics B* **30**, 1650234 (2016).
  - <sup>8</sup> Zhu, J.-J., Yao, D.-X., Zhang, S.-C. and Chang, K. *Physical review letters* **106**, 097201 (2011).
  - <sup>9</sup> Everschor-Sitte, K., Masell, J., Reeve, R. M. and Klau, M. *Journal of Applied Physics* **124**, 240901 (2018).
  - <sup>10</sup> Dai, Y. et al. *Physical Review B* **88**, 054403 (2013).
  - <sup>11</sup> Back, C. et al. *Journal of Physics D: Applied Physics* **53**, 363001 (2020).
  - <sup>12</sup> Kang, J. and Zang, J. *Physical Review B* **91**, 134401 (2015).
  - <sup>13</sup> Muhlbauer, S. et al. *Science* **323**, 915–919 (2009).
  - <sup>14</sup> Bernevig, B. A., Orenstein, J. and Zhang, S.-C. *Physical review letters* **97**, 236601 (2006).
  - <sup>15</sup> Koralek, J. D. et al. *Nature* **458**, 610–613 (2009).
  - <sup>16</sup> Noam Morali, Rajib Batabyal, Pranab Kumar Nag, Enke Liu, Qiunan Xu, Yan Sun, Binghai Yan, Claudia Felser, Nurit Avraham, Haim Beidenkopf, *Science*, **365**, 1286 (2019) DOI: 10.1126/science.aav2334
  - <sup>17</sup> Myung-Geun Han, Joseph A. Garlow, Yu Liu, Huiqin Zhang, Jun Li, Donald DiMarzio, Mark W. Knight, Cedomir Petrovic, Deep Jariwala and Yimei Zhu, *Nano Lett.*, **19**, **11**, 7859–7865 (2019).
  - <sup>18</sup> Bei Ding, Zefang Li, Guizhou Xu, Hang Li, Zhipeng Hou, Enke Liu, Xuekui Xi, Feng Xu, Yuan Yao, and Wenhong Wang, *Nano Lett.*, **20**, 868 (2020).
  - <sup>19</sup> Giang D. Nguyen, Jinhwan Lee, Tom Berlijn, Qiang Zou, Saban M. Hus, Jewook Park, Zheng Gai, Changgu Lee, and An-Ping Li, *Physical Review B* **97**, 014425 (2018).
  - <sup>20</sup> Yasufumi Araki, *Ann. Phys. (Berlin)*, **532**, 1900287, 1–16 (2020).
  - <sup>21</sup> P.K. Das, D.D. Sante, I. Vobornik, J. Fujii, T. Okuda, E. Bruyer, A. Gyenis, B.E. Feldman, J. Tao, R. Ciancio, G. Rossi, M.N. Ali, S. Picozzi, A. Yazdani, G. Panaccione, and R.J. Cava, *Nature Comm.* **7**, 10847 (2016).
  - <sup>22</sup> B. Feng, Y.-H. Chan, Y. Feng, R.-Y. Liu, M.-Y. Chou, K. Kuroda, K. Yaji, A. Harasawa, P. Moras, A. Barinov, W. Malaeb, C. Bareille, T. Kondo, S. Shin, F. Komori, T.-C. Chiang, Y. Shi, and I. Matsuda, *Phys Rev B* **94**, 195134 (2016).
  - <sup>23</sup> D. A. Pshenay-Severin, Y. V. Ivanov, A. A. Burkov, A. T. Burkov, *Journal of Physics: Condensed Matter* **30**, 135501 (2018).
  - <sup>24</sup> Su-Yang Xu, Ilya Belopolski, Daniel S. Sanchez, Madhab Neupane, Guoqing Chang, Koichiro Yaji, Zhujun Yuan, Chenglong Zhang, Kenta Kuroda, Guang Bian, Cheng Guo, Hong Lu, Tay-Rong Chang, Nasser Alidoust, Hao Zheng, Chi-Cheng Lee, Shin-Ming Huang, Chuang-Han Hsu, Horng-Tay Jeng, Arun Bansil, Titus Neupert, Fumio Komori, Takeshi Kondo, Shik Shin, Hsin Lin, Shuang Jia, M. Zahid Hasan, *Phys. Rev. Lett.* **116**, 096801 (2016).
  - <sup>25</sup> S. Varotto, L. Nessi, S. Cecchi, J. Ślawińska, P. Noël, S. Petrò, F. Fagiani, A. Novati, M. Cantoni, D. Petti, E. Albisetti, M. Costa, R. Calarco, M. Buongiorno Nardelli, M. Bibes, S. Picozzi, J.-Ph. Attané, L. Vila, R. Bertacco and Ch. Rinaldi, *Nature Electronics*, **4**, 740–747 (2021).
  - <sup>26</sup> S. Picozzi, *Frontiers in Physics. Condensed Matter Physics*, Vol.2, **10** (2014).
  - <sup>27</sup> N.N. Orlova, A.V. Timonina, N.N. Kolesnikov, E.V. Deviatov, *Physica B: Condensed Matter* **647**, 414358 (2022), <https://doi.org/10.1016/j.physb.2022.414358>
  - <sup>28</sup> Domenico Di Sante, Paolo Barone, Riccardo Bertacco, and Silvia Picozzi, *Adv. Mater.*, **25**, 509–513 (2013).
  - <sup>29</sup> Marcus Liebmann, Christian Rinaldi, Domenico Di Sante, Jens Kellner, Christian Pauly, Rui Ning Wang, Jos Emiel Boschker, Alessandro Giussani, Stefano Bertoli, Matteo Cantoni, Lorenzo Baldrati, Marco Asa, Ivana Vobornik, Giancarlo Panaccione, Dmitry Marchenko, Jaime Sánchez-Barriga, Oliver Rader, Raffaella Calarco, Silvia Picozzi, Riccardo Bertacco, Markus Morgenstern, *Adv. Mater.* **28**, 560 (2016)
  - <sup>30</sup> J. Krempaský, H. Volfová, S. Muff, N. Pilet, G. Landolt, M. Radović, M. Shi, D. Kriegner, V. Holý, J. Braun, H. Ebert, F. Bisti, V. A. Rogalev, V. N. Strocov, G. Springholz, J. Minár, and J. H. Dil, *Phys. Rev. B* **94**, 205111 (2016)
  - <sup>31</sup> A. Lau and C. Ortix, *Phys. Rev. Lett.* **122**, 186801 (2019)
  - <sup>32</sup> Juraj Krempaský, Laurent Nicolaï, Martin Gmitra, Houke Chen, Mauro Fanciulli, Eduardo B. Guedes, Marco Caputo, Milan Radović, Valentine V. Volobuev, Ondrej Caha, Gunther Springholz, Jan Minár, and J. Hugo Dil, *Phys.*

- Rev. Lett. 126, 206403 (2021)
- <sup>33</sup> N. N. Orlova, A. V. Timonina, N. N. Kolesnikov, and E. V. Deviatov Chinese Physics Letters 40, 077302 (2023) <https://doi.org/10.1088/0256-307X/40/7/077302>
- <sup>34</sup> Inti Sodemann, Liang Fu., Phys. Rev. Lett. 115, 216806 (2015)
- <sup>35</sup> G. Kremer, T. Jaouen, B. Salzmann, L. Nicolai, M. Rumo, C. W. Nicholson, B. Hildebrand, J. H. Dil, J. Minár, G. Springholz, J. Krempaský, and C. Monney, Phys. Rev. Research 2, 033115 (2020).
- <sup>36</sup> Ch. Rinaldi, S. Varotto, M. Asa, J. Sławinska, J. Fujii, G. Vinai, S. Cecchi, D. Di Sante, R. Calarco, I. Vobornik, G. Panaccione, S. Picozzi and R. Bertacco, Nano Lett., 18, 2751–2758 (2018).
- <sup>37</sup> A.A. Avakyants, N.N. Orlova, A.V. Timonina, N.N. Kolesnikov, E.V. Deviatov, Journal of Magnetism and Magnetic Materials, 573, 170668 (2023), <https://doi.org/10.1016/j.jmmm.2023.170668>.
- <sup>38</sup> N. N. Orlova, A. A. Avakyants, A. V. Timonina, N. N. Kolesnikov, and E. V. Deviatov, Phys. Rev. B 107, 155137 (2023), <https://doi.org/10.1103/PhysRevB.107.155137>
- <sup>39</sup> Coey, J. M. D. Magnetism and Magnetic Materials; Cambridge University Press, 2009.
- <sup>40</sup> Kelly, P. E.; O'Grady, K.; Mayo, P. I.; Chantrell, R. W. IEEE Trans. Magn. 25, 3881 (1989).
- <sup>41</sup> Henkel, O. Phys. Status Solidi B 7, 919 (1964).
- <sup>42</sup> Bender, P.; Krämer, F.; Tschöpe, A.; Birringer, R., J. Phys. D: Appl. Phys. 48, 145003 (2015).
- <sup>43</sup> J. Sánchez, C. Sánchez, A. Gil Santana, J. Magn. Magn. Mater. 294, 226 (2005)
- <sup>44</sup> J. E. Lewis, Phys. Status Solidi 38, 131 (1970).
- <sup>45</sup> C. Israel, S. Kar-Narayan, and N. D. Mathur, Applied Physics Letters 93, 173501 (2008)
- <sup>46</sup> Zhong Shen, Shuai Dong, and Xiaoyan Yao, arXiv:2310.04810 (2023).
- <sup>47</sup> Adolfo O. Fumega and J. L. Lado, 2D Materials 9, 025010 (2022). <https://doi.org/10.1088/2053-1583/ac4e9d>
- <sup>48</sup> Vincensius Gunawan, Ngurah Ayu Ketut Umiati, International Journal of Electrical and Computer Engineering (IJECE), 8, 4823 (2018). DOI: 10.11591/ijece.v8i6.pp4823-4828